Mechanism of Ta on the microstructure and properties of Fe-Mn damping alloys

Gui-Xiang Liu[a], Kun Zhang[a], Chao Han[a], Xiao-Lin Shao[a], Jun Lu[a], Lin Zhang[b,c], Xiao-Song Jiang[b,c]*(ID) , Zi-Xuan Wu[d], Liu Yang[e]

[a]The Second Sub-Institute, Nuclear Power Institute of China, Chengdu 610005, China

[b]Key Laboratory of Advanced Technologies of Materials, Ministry of Education, Chengdu 610031, China

[c]School of Materials Science and Engineering, Southwest Jiao tong University, Chengdu 610031, China

[d]School of Engineering and Materials Science, Queen Mary University of London, London E1 4NS, United Kingdom

[e]Institute for Applied Materials (IAM-WK), Karlsruhe Institute of Technology (KIT), Karlsruhe 76131, Germany

*Corresponding author: xsjiang@swjtu.edu.cn (Xiao-Song Jiang); Tel./Fax: +86-28-87634177.

Abstract Fe-Mn-Co-*x*Ta alloys (*x*=0, 1, 2, 3 wt.%) were fabricated using spark plasma sintering to explore the influence of Ta content on the microstructure, mechanical properties, and damping characteristics of Fe-17Mn-3Co damping alloys. The microstructural analysis reveals the dominant presence of γ-austenite, ε-martensite, α′-martensite, and Co_3Ta precipitates within the alloy. Incremental increments in Ta content exhibit proportional enhancements in hardness, tensile strength, and fracture elongation of the alloy. Notably, these improvements in mechanical attributes are closely correlated with the generated second-phase Co_3Ta. As the Ta content increases, there is a gradual augmentation in the formation of Co_3Ta within the alloy. Consequently, the damping property initially experiences an ascent followed by a subsequent decline with rising Ta content. This damping behavior finds its origins in multiple mechanisms, including grain boundary damping stemming from reduced grain size, interfacial damping induced by the generated Co_3Ta, and dislocation damping. It's noteworthy that the emergence of the secondary phase wields a dual impact on damping property. On the one hand, the proliferation of the second phase fosters increased interfaces for energy dissipation. On the other hand, these interfaces give rise to compressive stresses, constraining interface movement and thus impeding damping property enhancement.

Keywords Fe-Mn-Co; Ta; spark plasma sintering; Mechanical properties; Damping

1. Introduction

In recent years, due to the increasing power and frequency of mechanical equipment, the vibration and noise generated by the equipment have an impact on the fatigue-resistant performance and service life of various instruments, and even cause harm to human health. [1-6]. Therefore, suitable approaches to vibration and noise reduction are needed. Designing materials with high damping property is a good approach. In comparison to alternative damping materials [3-6], extensive research has been conducted on Fe-Mn-based damping alloys due to their inherent benefits, including elevated strength, cost-effectiveness (merely one-fourth the cost of nonferrous damping alloys) [7], and an amplitude-dependent enhancement in damping property [8]. The mechanism of damping property formation is related to the interfacial motion, thermal motion, and dislocation effects within the alloy [9]. Fe-Mn-based alloys are a new type of damping materials with a typical transition process of γ-austenite to ε-martensite [10-12]. Current studies on damping mechanisms are mainly related to martensite and austenite [13-15]. However, the damping mechanisms of different Fe-Mn bases are quite different and need to be further explored. Besides, they have low damping property at low amplitude [14,15]. It has been shown that both heat treatment and alloying can affect the damping property [16-18]. Employing heat treatment has the potential to elevate the ε-martensite content, consequently leading to an augmentation of the damping property. However, subjecting the alloy to multiple thermal cycles of heat treatment not only diminishes its damping property but also moderately impairs its mechanical properties [17]. This presents a challenge for the alloy to fulfill the prerequisites of practical applications.

Modulating the Mn composition or introducing N, Co, and Ce constituents presents a viable strategy for enhancing damping property in Fe-Mn-based alloys [11,19-22]. The infusion of these alloying agents serves to heighten the abundance of ε-martensite, thereby concomitantly augmenting the population of damping sources [19-21]. Also, the introduction of a second phase provides more damping interfaces [21]. Moreover, Fe-Mn-based alloys showcase unique damping mechanisms stemming from ε-martensite metal complexation, alongside grain boundary, interfacial, dislocation, and hybrid damping effects akin to metal matrix composites [9,23]. Nevertheless, compounded alloys have the potential to instigate lattice distortions that impede the γ-austenite to ε-martensite phase transition, consequently resulting in a diminution of the damping property [24]. Furthermore, strategic alloying offers an avenue for enhancing the mechanical characteristics of the alloy [25]. A case in point is the discernible increase in tensile strength through the incorporation of Cr elements within the Fe-Mn-Co alloying matrix [26]. Experimental evidence underscores the introduction of a secondary phase via the integration of Ta elements into Cu-based alloys, manifesting in a concomitant reduction of grain size and augmentation of mechanical traits, coupled with a concurrent attenuation of damping effects [27]. Xu et al. constructed a dual-multiphase structure in CoCrNi medium-entropic alloys with the addition of Ta and a thermo-mechanical machining process, which greatly improved the strength and toughness [28]. In addition, it has been shown that the addition of Ta to ceramics can also improve the mechanical properties, mainly due to the refinement of ceramic particles, the reduction of voids, and the solid solution of Ta in the Ni binder and ceramic particles by the addition of Ta [29]. Significantly, the intricate ramifications of Ta elements upon the mechanical and damping facets intrinsic to Fe-Mn-Co-based alloys remain uncharted, hence propelling the imperative to unveil and elucidate the multifaceted effects of Ta elements upon both damping and mechanical attributes within the Fe-Mn-Co alloy matrix.

Hence, this study delves into the fabrication of a Fe-Mn-Co-Ta alloy featuring superior plasticity and elevated densities, yielding improvements in both mechanical and damping properties. Extensive analysis is devoted to the alloy's microstructure and mechanical attributes, coupled with a thorough investigation into the modulating influence exerted by Ta element addition upon the mechanical and damping characteristics of the Fe-Mn-Co alloy.

2. Experimental

Four kinds of powders, namely, iron powder, manganese powder, cobalt powder and tantalum powder with a purity of 99.9%, were selected as raw materials. The four powders were mixed according to specific ratios and ball-milled for 40 h. A certain amount of tert-butanol was added to prevent oxidation during the ball-milling process. After ball milling, the powders were freeze-dried for 24 h. Afterwards, the dried powders were sintered in an abrasive tool in an spark plasma sintering (SPS) machine (HPD25 from FCT, Germany). During the sintering process the samples were heated to 1000°C, pressurized to 40 MPa and held for 600 s. Finally the samples were cooled at room temperature. The experimental steps are shown in Fig. 1.

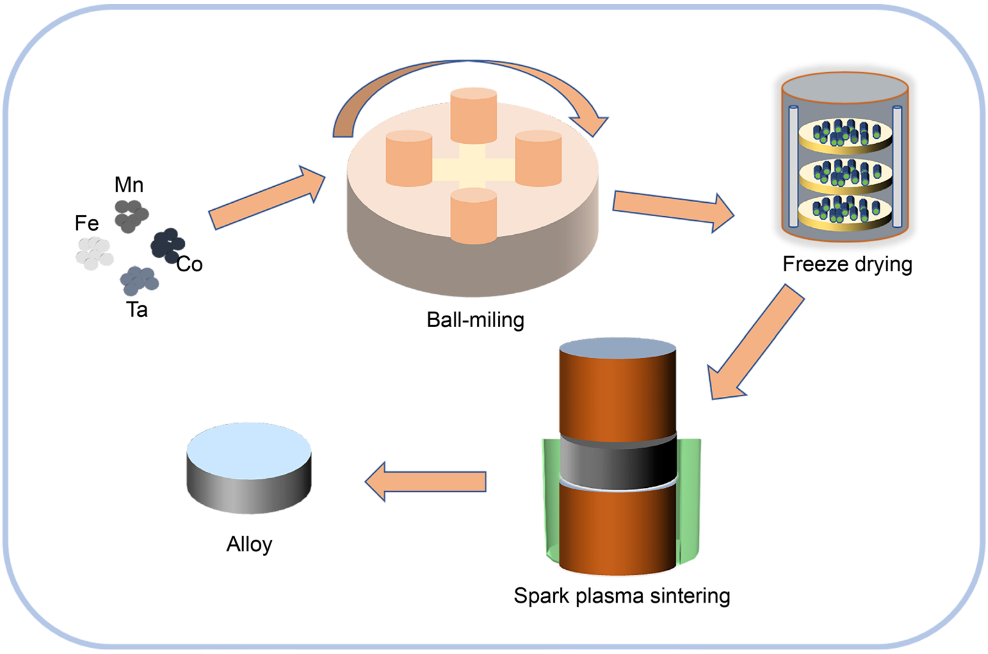

Fig.1 Flow chart for the preparation of Fe-Mn-Co-*x*Ta alloy.

The sintered samples were wire cut to specific dimensions. The cut samples were subjected to tensile testing at a velocity of 0.5 mm·min^{-1}. The dimension of the tensile sample was 36mm × 4mm × 2mm. The surface of the alloy was polished and the densities were tested. The surface hardness of the alloys was tested using a Vickers hardness tester (HXD-100TM/LCD, China) at a pressure of 1 kg for 15 s. The damping property of the alloys were tested using a multifunctional internal dissipation meter (MFP1000, China). The phases of the alloys were analyzed by X-ray diffraction (XRD, X-Pert Pro MPD Netherlands) at 40 kV and 20 mA. The alloys' surface and tensile fracture morphologies were analyzed utilizing scanning electron microscopy (SEM; JEOL JSM-7001F, German) and transmission electron microscopy (TEM; JEOL JEM-F200, Japan).

3.Results and Discussion

3.1 Microstructure characterization of alloys

In order to analyze the effect of Ta element content on the phase composition of Fe-17Mn-3Co alloy, X-ray diffraction analysis was performed. The graphical representation of X-ray diffraction (XRD) outcomes, as depicted in Fig. 2, offers insight into the alloy's primary constituents, namely, γ-austenite, ε-martensite, and α′-martensite. During rapid cooling of the SPS, γ-austenite to ε-martensite, ε-martensite to α′-martensite and γ-austenite to α′-martensite transformations may occur, resulting in the appearance of three phases in the XRD. Remarkably, α′-martensite and ε-martensite are stable phases with body-centered tetragonal structure, which can increase the strength of alloys [30]; however, it is worth underscoring that this particular phase remains void of any influence over the alloy's damping characteristics [31]. As the Ta element content escalates, the intensity of the $(0002)_\varepsilon$ peak in the ε-martensite phase consistently rises, while the $(111)_\gamma$ peak corresponding to the γ phase remains virtually invariant; however, a gradual attenuation is discernible in the magnitude of the $(022)_\gamma$ peak. Simultaneously, the α′ peak, representative of α′-martensite, exhibits augmentation congruent with the augmentation of Ta content. These observations collectively underscore the role of Ta incorporation in diminishing the driving impetus of ε-martensite transformation [18], thereby engendering an amplification in the ε-martensite content. Besides, a small number of peaks of the Co_3Ta phase appeared in the 2Ta and 3Ta alloys as the Ta content increased. However, the absence of peaks of the Co_3Ta phase in 1Ta alloys may be due to the low content that was not scanned by XRD [32]. It was shown that refining the grains also reduces the intensity of the diffraction peaks [33]. Therefore, $(111)_{\gamma}$,$(0002)_{\varepsilon}$,$(10\bar{1}1)_{\varepsilon}$,$(200)_{\gamma}$,$(211)_{\alpha'}$ were selected in the XRD plots to obtain the average grain sizes of the four alloys by the Scherrer formula as shown in Table 1. The findings indicate a fluctuating pattern in grain size as the Ta content varies. Specifically, the grain size diminishes initially, followed by an increase. However, the reason for the absence of peaks of the Co_3Ta phase in the 1Ta alloy may be due to the fact that the content is too low to be scanned by XRD. In addition, a small number of peaks of MnO appeared in all four alloys. This is produced by the extreme susceptibility of Mn to oxidation [18].

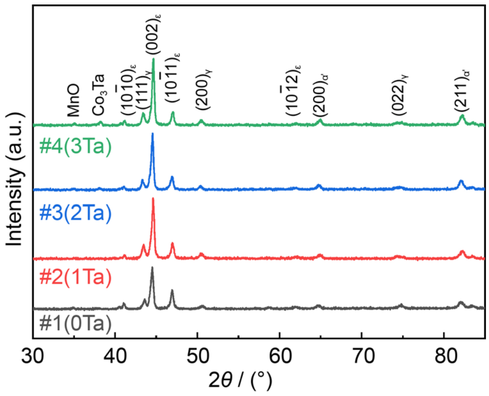

Fig.2 XRD patterns of Fe-Mn-Co-*x*Ta alloys.

Table 1 The average grain size and strain of the samples were estimated by Jade software.

Materials	Average grain size/nm
0Ta	34.8 ± 2
1Ta	26.5 ± 3
2Ta	28.7 ± 4
3Ta	32.0 ± 4

The microstructural features of Fe-Mn-Co-*x*Ta alloys at distinct Ta compositions are visually captured in the SEM images of Fig. 3. The variation of grain size is not clearly visible in Fig. 3, which may be caused by the small extent of grain size variation. However, in combination with Table 1, it is known that the grain size varies with the increase of Ta. In Fig. 3a, it can be seen that more MnO appears on the surface of the alloy without Ta elements, and the Fe-Mn matrix phase is uniformly distributed without the precipitation phase. After the addition of the Ta element, in Fig. 3b, in addition to the presence of MnO, a bulge occurred on the surface of the matrix, and a Ta-rich phase was generated on the surface of the matrix (point 2). We found that the composition of the Ta-rich phase is Co_3Ta by energy dispersive spectroscopy (EDS) analysis, which is consistent with the results of XRD in Fig. 2. As demonstrated in Fig. 3c, the introduction of additional Ta elements serves to mitigate substrate surface oxidation while concurrently augmenting the Co_3Ta concentration. Upon reaching a Ta content of 3 wt.%, the surface bulge observed on the alloy disappears, leading to a smoother matrix, and facilitating further growth of the Co_3Ta phase. The inclusion of Ta triggers a reaction with Co, culminating in the formation of the Co_3Ta phase. This phenomenon arises primarily due to the disparate crystal structures of Co (hexagonal) and Ta (body-centered cubic), which exhibit near-insolubility within the solid state. And the reason that the Ta atom has a large difference in radius from Fe, Mn and Co makes the solubility between Ta and Fe, Mn and Co elements poor, thus forming the Co_3Ta second phase. Moreover, a gradual reduction in the degree of oxidation is observed concomitant with the increasing Ta content, highlighting the inhibitory influence exerted by the incorporation of Ta on oxide development, thus resulting in an augmentation of oxidation resistance [34,35].

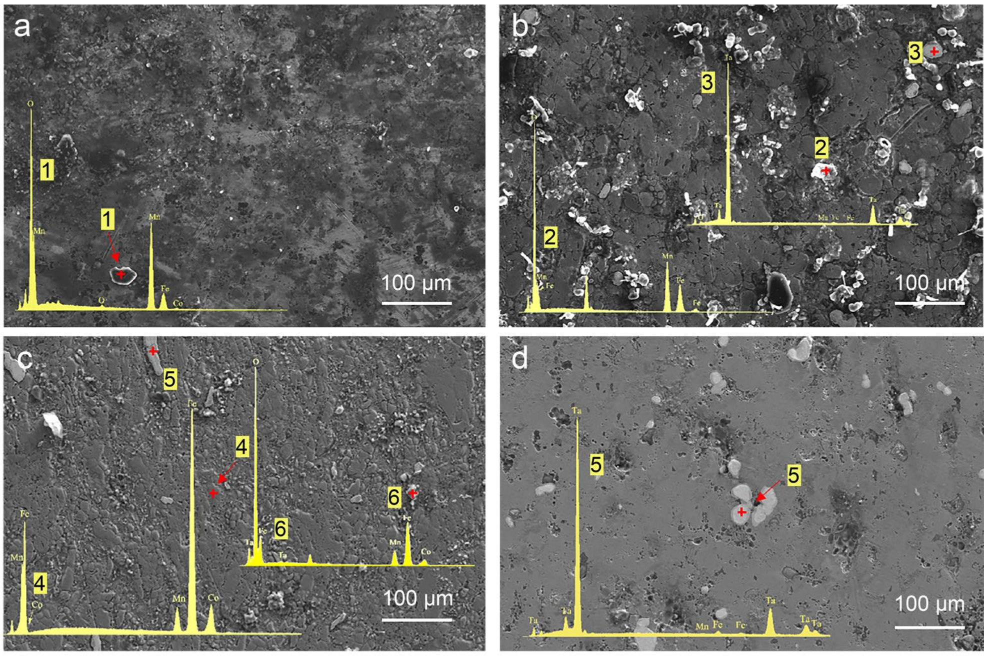

Fig.3 SEM images of Fe-Mn-Co-*x*Ta alloys. **a** 0Ta; **b** 1Ta; **c** 2Ta; **d** 3Ta

To validate the elemental distribution within the alloy containing 2 wt.% Ta, a surface scanning analysis was conducted, as depicted in Fig. 4. The images in Fig 4b-f reveal a notably even dispersion of the Fe-Mn-Co elements, while the Ta-rich phase demonstrates a uniform presence across the matrix surface. The surface scan analysis shows that the raised part is the matrix, and the main components are Fe and Mn elements. In addition, it is also demonstrated from the face sweep that the alloy prepared by SPS sintering can promote close particle contact [36], which reduces porosity and shrinkage and helps to improve the mechanical properties.

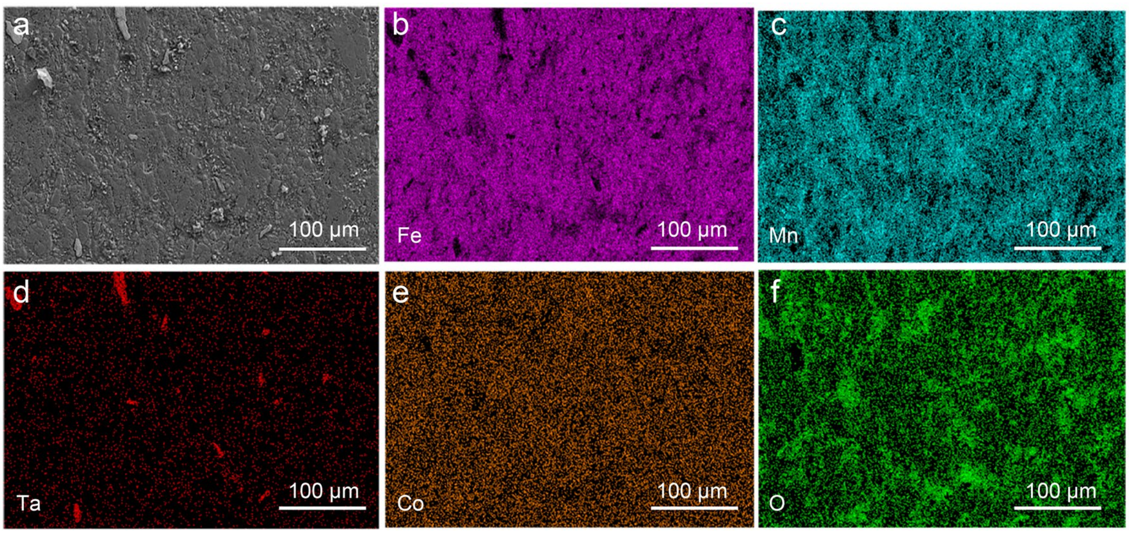

Fig.4 a Scanning electron microscope images of Fe-17Mn-3Co-2Ta alloy; **b-f** distribution of different elements on the surface

Through a TEM analysis, the internal organization distribution of the alloy was scrutinized. The TEM bright field image and selected area electron diffraction (SAED) spectrum, as depicted in Fig. 5, reveal a profusion of interwoven dislocation lines within the Fe-17Mn-3Co-2Ta alloy (Fig. 5a,b). This intricate dislocation network is the outcome of the deformation caused by the collision of high-energy spheres with the alloy powder during preliminary ball milling. In the subsequent SPS sintering, a large number of dislocations were retained inside the alloy due to rapid cooling [37]. Moreover, the Co_3Ta phase (point A) is seen in Fig. 5c near the dislocation clusters (point B), which accumulate at the grain boundaries. And point C is found to be mainly the Fe-Mn matrix by EDS energy spectrum analysis. Their SAED spectra are outlined in Fig. 5d-f.

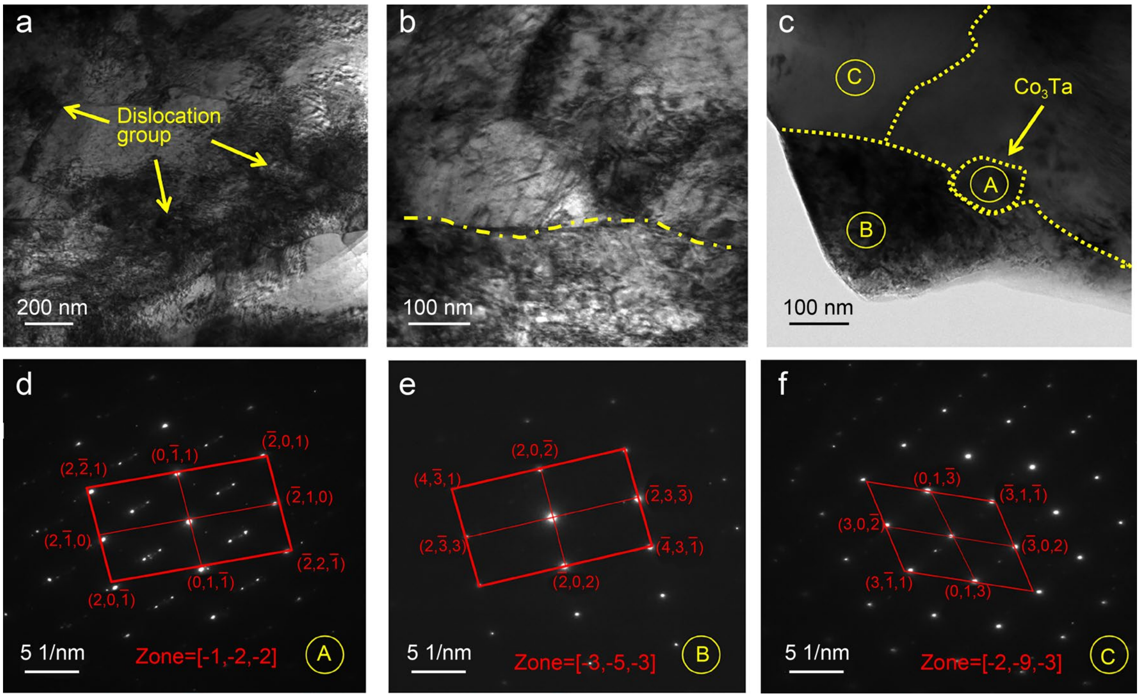

Fig.5-a-c TEM bright-field plots of different regions within the Fe-Mn-Co-2Ta alloy; **d-f** SAED spectra corresponding to regions A, B, and C in **c**

3.2 Mechanical properties of alloys

The practical application of composites is directly dependent on their mechanical properties, of which the density of powder metallurgy sintered composites is a key performance benchmark. Using Archimedes' principle, density measurements were carried out and the experimental results are shown in Fig. 6. The Fe-17Mn-3Co alloy has the highest relative density of about 98.5%, and Fe-Mn-Co-2Ta has the next highest relative density of 98.1%. With the increase of Ta content, the trend of relative density of the alloys increases and then decreases. It can be seen that the relative density of the alloys generally remains at a high level with the addition of Ta. The addition of Ta has little effect on the densification of the Fe-Mn-Co based composites. SPS sintering, on the other hand, inhibits grain growth through rapid temperature increase, thus increasing the density of the alloy[38].

Table 2 Mechanical properties of Fe-Mn-Co-*x*Ta alloy

Alloy/wt.%	Tensile strength / MPa	Fracture elongation / %	Hardness / HV
Fe-Mn-Co	200.8	3.1	283.3±10.3
Fe-Mn-Co-1Ta	289.2	13.1	297.7±2.87
Fe-Mn-Co-2Ta	336.9	18.0	303.6±3.42
Fe-Mn-Co-3Ta	393.9	23.6	322.2±2.27

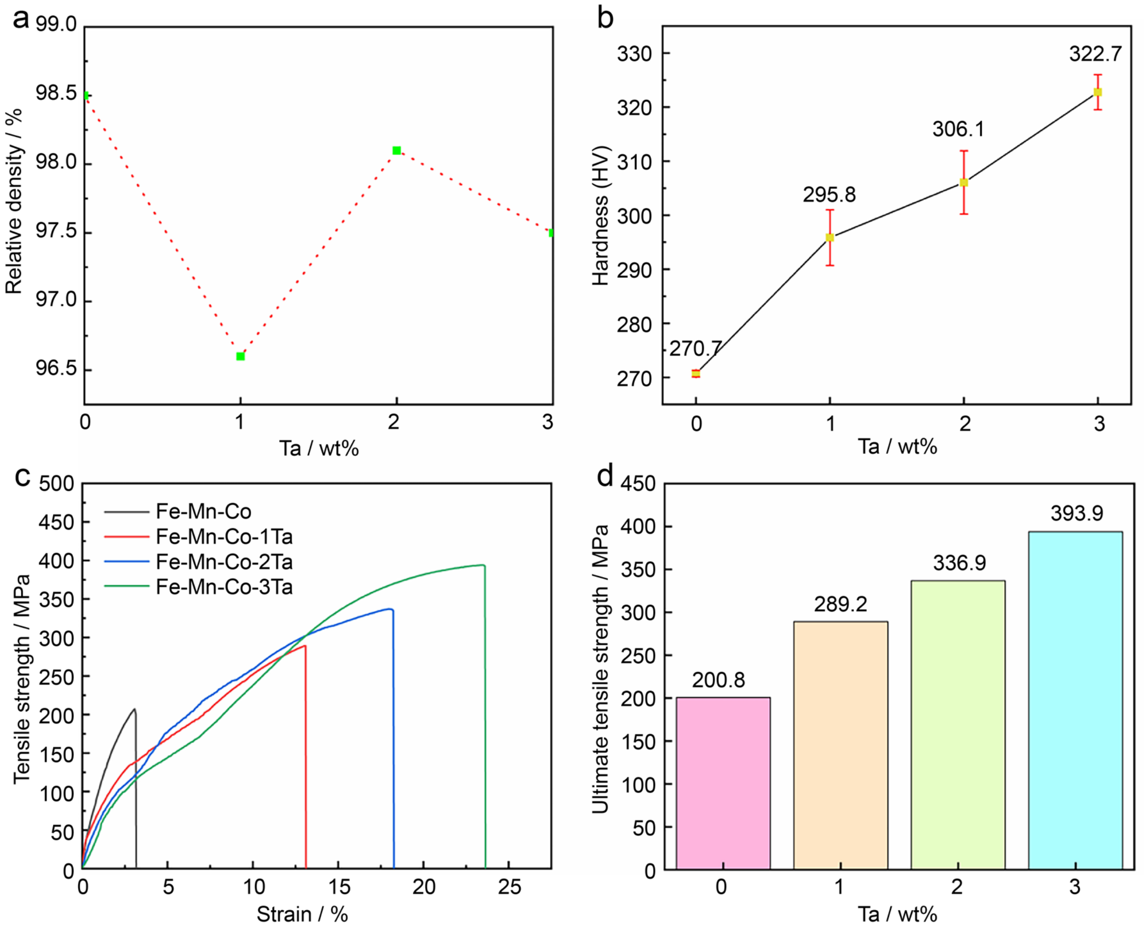

Fig.6 Mechanical properties of Fe-Mn-Co-*x*Ta alloy **a** Densities of the alloy; **b** Hardness of the alloy; **c** Stress-strain curve of the alloy; **d** Tensile strength of the alloy

Table 2 presents the mechanical characteristics of the alloys across distinct Ta compositions at room temperature. Figure 6b-d displays corresponding graphs derived from the data in Table 1, elucidating the alloy behaviors. As evident from Figs. 6b, c, the variations in hardness and tensile strength closely mirror the trajectory observed with ascending Ta content. A closer look unveils the Fe-17Mn-3Co alloy's tenacity, embodying a hardness of 283.3 HV, a tensile strength of 200.8 MPa, and a fracture elongation of 3.1%. The crescendo, however, emerges with the integration of 3 wt.% Ta into the Fe-17Mn-3Co-3Ta alloy, invoking an astounding transformation that escalates hardness, tensile strength, and fracture elongation by 13.7%, 96.2%, and an awe-inspiring 661.3%, respectively. The quintessential embodiment of mechanical prowess emerges resoundingly in the Fe-Mn-Co-3Ta alloy. This flagship alloy robustly substantiates the strategic integration of Ta, instigating a profound overhaul in mechanical attributes. This transformative voyage is choreographed by the harmonious choreography of two fundamental protagonists: the elegance of fine-grain strengthening, triggered by meticulous grain size reduction, and the catalytic sway of Co_3Ta second-phase precipitation strengthening. This nuanced interplay, meticulously woven through the revelations of Figs. 3, 4, crystallizes in intriguing clarity. The infusion of 1 wt.% Ta galvanizes a sequence of metamorphoses: an attenuated grain size bestows renewed impetus upon internal interfaces, a milieu wherein the congregation of dislocations flourishes. In this meticulously orchestrated narrative, the fine-grain strengthening takes center stage, an orchestrator of mechanical augmentation par excellence. In addition, a small amount of the Co_3Ta phase also starts to be formed, and the Co_3Ta phase also plays a role in pinning down dislocations and impeding dislocation movement. Further increasing the content of Ta elements, the internal grain size of the alloy increases, and the fine grain strengthening effect decreases, at which time the precipitation strengthening effect plays a major role. With the increase of Ta content, more Co_3Ta

phases are generated inside the alloy. Along with the increase of the Co_3Ta phase, the pinning effect on dislocations also gradually increases. In addition, the Co_3Ta phase also grows and aggregates, impeding the movement of dislocations, as shown in point 5 in Fig. 3d. In addition, the TEM image shows that the Co_3Ta phase hinders the motion of dislocations, which further increases the strength and hardness of the dislocations by aggregation at the grain boundaries.

A compelling revelation emerges upon the infusion of 3 wt.% Ta, unfurling a remarkable surge in plasticity, an accomplishment realized even in the absence of fine-grain strengthening's influence. The SEM morphology of the tensile fracture surface within the Fe-Mn-Co-*x*Ta damping alloy is illustrated in Fig. 7. The fracture behavior exhibited by the alloy is distinctly indicative of ductile fracture, discerned from the features of the fracture micrograph. Specifically, Fig. 7d vividly illustrates that the Fe-Mn-Co-3Ta alloy manifests the most pronounced concentration and depth of toughness pockets, which exhibits a strong correlation with escalated tensile strength and fracture elongation values. This elucidates the trend wherein the incorporation of Ta elements corresponds to an augmentation in the count of ductile tough inclusions within the alloy, ultimately contributing to an elevation in tensile strength and the manifestation of plastic fracture characteristics. Furthermore, apart from the evident presence of toughness pockets in the SEM fracture image of the Fe-Mn-Co-3Ta alloy, an associated crack is discernible, as highlighted in Fig. 8. The figure shows a crack through the Co_3Ta phase, which indicates that the matrix begins to fracture during the stretching process. When the crack passes through to the Co_3Ta phase, load transfer occurs due to the fact that Co_3Ta is softer compared to the matrix. The crack was transferred on the matrix to the interior of the Co_3Ta phase. With the gradual increase in stress, the crack continues to transfer in the Co_3Ta phase until fracture. Furthermore, it can be seen that several cracks occurred in the Co_3Ta phase in Fig. 7d. This indicates that the cracks pass through these ductile, hard inclusions of the Co_3Ta phase during stretching increases the elongation by adding more fracture surfaces . Besides, A thorough energy-dispersive spectroscopy analysis conducted on both sides of the crack conclusively indicates its traversal through the Co_3Ta phase, characterized by minor Fe and Mn constituents. This Co_3Ta phase is found adjacent to a Fe and Mn solid solution based on Fe. To further confirm the cause of crack formation, a face scan analysis of the fracture of Fe-Mn-Co-3Ta alloy was performed as shown in Fig. 9. The findings elucidate a discernible non-uniformity in element distribution throughout the fracture progression, ultimately culminating in the genesis of a crack resultant from the fracture of the Co_3Ta second phase. A large amount of Co_3Ta is also present around the crack, and since the second phase strengthening and pegging of dislocations are stronger than the formation and growth of the crack, the strength and toughness of the material can be improved at the same time when the Ta content is in a certain range[39]. In addition, it was shown that the Ta element itself has good ductility, and the Co_3Ta generated with the Co element also has excellent plasticity [40], and the combined effect with the second-phase strengthening makes the plasticity of Fe-17Mn-3Co-3Ta alloy substantially improved.

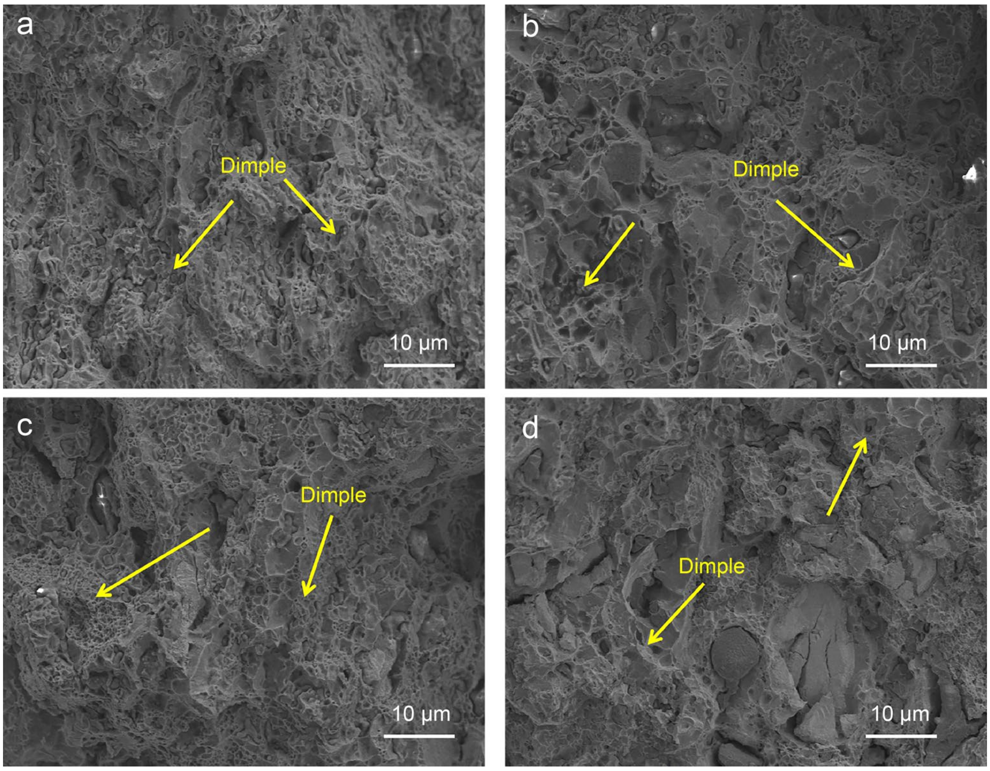

Fig.7 SEM images of tensile fractures. **a** Fe-Mn-Co; **b** Fe-Mn-Co-1Ta; **c** Fe-Mn-Co-2Ta; **d** Fe-Mn-Co-3Ta

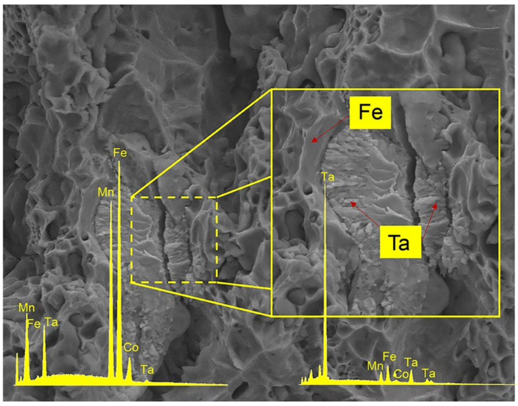

Fig.8 Fracture SEM image of Fe-Mn-Co-3Ta alloy.

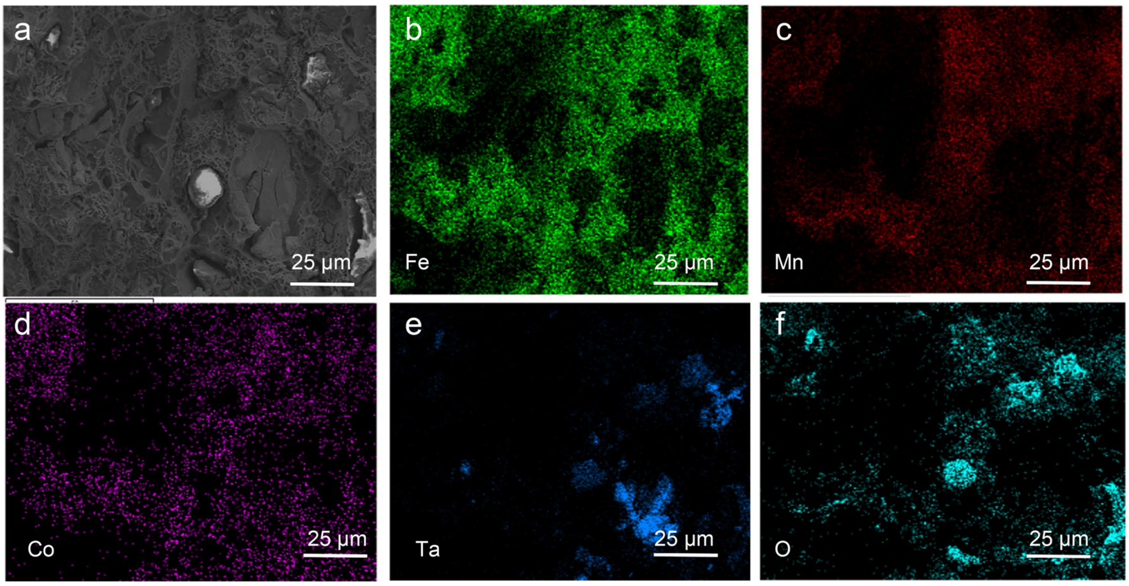

Fig.9 SEM images of Fe-Mn-Co-3Ta **a** fracture morphology; **b-f** EDS surface scans of the fractures.

3.3 Damping property of alloys

The relationship between strain amplitude and the damping property of the Fe-Mn-Co-*x*Ta alloy is elucidated in Fig. 10. Notably, the damping characteristics of all the alloys exhibit an upward trajectory concomitant with amplified strain amplitudes. Particularly, the damping property shifts with a more gradual tempo under lower strain amplitudes. However, as strain amplitudes escalate, the alloy manifests a propensity for interfacial motion within structural imperfections, including the second phases and dislocations. This orchestrated interplay contributes to heightening energy dissipation, thereby augmenting the alloy's damping efficacy [27]. The influence of Ta emerges as a pivotal factor impacting damping property; an ascent followed by a descent characterizes the relationship between damping property and Ta content. Among the alloys, Fe-Mn-Co-2Ta alloy ascends to the zenith with a damping property of 0.027, while the nadir is occupied by Fe-Mn-Co alloy, showcasing a minimal damping property of 0.014. Therefore, the addition of Ta leads to a significant increase in the damping property of the alloy.

The incorporation of Ta within the alloy significantly influences its damping characteristics, primarily orchestrated through the modulation of grain size and the generation of Co_3Ta, thus engendering grain boundary and interfacial damping effects. This phenomenon is evident in the results of Table 1, where the introduction of 1 wt.% Ta leads to an initial reduction in the alloy grain size compared to the results without Ta. This reduction amplifies the expanse of pliable grain boundaries, thereby amplifying the avenue for energy dissipation. With the further addition of Ta, the grain size increases with increasing Ta content, while many Co_3Ta grains are formed that are different from the matrix type. In this case, although the grain boundary area available for energy dissipation decreases, the Co_3Ta phase formed increases. The formation of the second phase inside the alloy has good plasticity and can dissipate some energy so that the energy originally used for fracture can be used for damping. In addition, with the increase of the Co_3Ta phase, Co_3Ta is diffusely distributed within the alloy to pin to dislocations, which hinders the movement of dislocations, and at the same time increases the energy dissipated in the movement of the interface and improves the damping property of the alloy. However, When the Ta content is elevated to 3 wt.%, the alloy exhibits an enlargement in grain size, coupled with a reduction in the mobility of grain boundaries. This coincides with a notable rise in the concentration of Co_3Ta within the alloy matrix. The heightened Co_3Ta content substantially impedes the motion of dislocations, effectively immobilizing them, particularly under conditions of elevated strain amplitude. Consequently, this results in a discernible reduction in the damping propensity of the material. Interestingly, at a Ta content of 3 wt.%, the damping behavior of the alloy closely resembles that of the 1 wt.% counterpart. It is noteworthy that the optimal damping property is realized when the Ta content is maintained at 2 wt.%. This is because the Co_3Ta content is so small after adding 1wt.% Ta that the damping property is improved only by the grain boundary damping effect due to grain refinement. Introduction of 3 wt.% Ta leads to pronounced growth and aggregation of Co_3Ta content, accompanied by a consequential enlargement in grain size, thereby inducing a decrement in damping attributes. When the Ta content is stabilized at 2 wt.%, the resultant grain size approximates that of the 1 wt.% Ta variant, thus facilitating optimal damping property through the synergistic interplay of grain boundary and interfacial damping mechanisms instigated by Co_3Ta. In summary, the influence of Ta on the alloy's damping characteristics is manifest through its modulation of phase composition, grain size, and their collective impact on grain boundaries.

Moreover, an inherent dislocation damping mechanism operates within the alloy, showcasing amplitude-dependent tendencies. This observation is substantiated through transmission electron microscopy imaging, which exposes a profusion of dislocation lines originating predominantly from ball milling process. It induces plastic deformation and inter-powder collisions, thereby engendering a substantial population of dislocations, which persist throughout subsequent spark plasma sintering. It is pertinent to note that dislocation mobility undergoes modulation in correspondence with altering amplitudes, as evidenced in prior investigations [8]. Figure 10 provides visual insight into the intricate interplay between the incorporation of 2 wt.% Ta and the resultant damping property of the alloy, with specific emphasis on the amplitude parameter. Significantly, a substantial enhancement in damping effectiveness manifests as the amplitude exceeds the value of 600×10^{-6}. This enhancement can be attributed to the attainment of a critical amplitude threshold, facilitating the liberation of dislocations from the restraining effects imposed by the Co_3Ta phase. As a consequence, dislocations are rendered capable of traversing, leading to heightened energy dissipation.

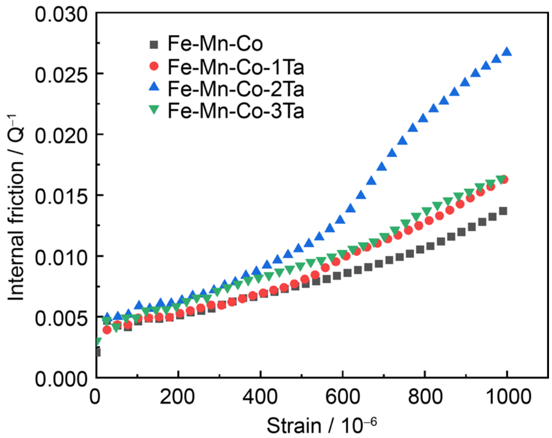

Fig.10 Room temperature damping property of Fe-Mn-Co-*x*Ta alloys.

4. Conclusion

Mechanical alloying followed by spark plasma sintering was employed for the fabrication of Fe-Mn-Co-Ta alloys. Introduction of Ta into Fe-17Mn-3Co alloys yields discernible enhancements in mechanical attributes. The observed rise in both strength and plasticity with increasing Ta content is attributed to the cooperative influence of fine-grain strengthening and second-phase reinforcement mechanisms. The substantial enhancement in plasticity can be attributed to the emergence of the Co_3Ta second phase. In addition, the addition of Ta gives the alloy better damping property compared to the alloy without Ta. The damping property of the alloys exhibit an initial increase followed by a subsequent decrease in response to elevated Ta content. This damping behavior is predominantly influenced by three key factors: the damping effect associated with grain boundary modifications resulting from grain refinement, the interface damping effect, and the dislocation damping effect stemming from the formation of the Co_3Ta second phase. The presence of this second phase induces a dual influence on the damping property. Initially, the introduction of the second phase contributes to energy dissipation, thereby enhancing interfacial interactions and augmenting the overall damping propensity. However, as the size and abundance of the second phase increase, it imparts a more pronounced pinning effect on dislocations, consequently attenuating the dislocation damping effect.

Acknowledgments

This work was supported by the Key Laboratory of Infrared Imaging Materials and Detectors, Shanghai Institute of Technical Physics, Chinese Academy of Sciences (No. IIMDKFJJ-21-10) and China Postdoctoral Science Foundation (No. 2018T110993).

Declarations

Conflict of interest The authors declare that they have no conflict of interest.

Data Availability statement

The data used to support the findings of this study are available from the corresponding author upon reasonable request.

References

[1]Mou XX, Li N, Yan JZ. Investigation of constant prestress in effecting damping capacity of Fe-15Cr-2.5Mo-1.0Ni casting ferromagnetic alloy. J Alloy Compd. 2015;650:92. http://dx.doi.org/10.1016/j.jallcom.2015.07.273

[2]Yan SH, Li N, Wang J, Yan JZ, Liu WB, Li D, Mou XX, Ying L, Zhao XC. Effect of minor Zr element on microstructure and properties of Fe-16Cr-2.5Mo damping alloys. J Alloy Compd. 2018;740:587. https://doi.org/10.1016/j.jallcom.2017.11.354

[3]Sun M, Balagurov A, Bobrikov I, Wang XP, Wen W, Golovin IS, Fang QF. High damping in Fe-Ga-La alloys: Phenomenological model for magneto-mechanical hysteresis damping and experiment. J Mater Sci Technol. 2021;72:69. https://doi.org/10.1016/j.jmst.2020.07.043

[4]Gómez-Cortés JF, Fuster V, Pérez-Cerrato M, Lorenzo P, Ruiz-Larrea I, Breczewski T, Nó ML, San Juan JM. Superelastic damping at nanoscale in ternary and quaternary Cu-based shape memory alloys. J Alloy Compd. 2021;883:160865. https://doi.org/10.1016/j.jallcom.2021.160865

[5]Wang W, Yi DQ, Hua W, Wang B. High damping capacity of Al-40Zn alloys with fine grain and eutectoid structures via Yb alloying. J Alloy Compd. 2021;870:159485. https://doi.org/10.1016/j.jallcom.2021.159485

[6]Liu ZL, Liu XQ, Shen P, Zhu XR, Meng L. Effect of ball-milling parameter on mechanical and damping properties of sintered Mg-Zr alloy. T Nonferr Metal Soc. 2010;20(11):2092. https://doi.org/10.1016/S1003-6326(09)60423-4

[7]Huang SK, Wen YH, Li N, Teng J, Ding S, Xu YG. Application of damping mechanism model and stacking fault probability in Fe-Mn alloy. Mater Charact. 2008;59(6):681. https://doi.org/10.1016/j.matchar.2007.05.023

[8]Huang SK, Huang WR, Liu JH, Teng J, Li N, Wen YH. Internal friction mechanism of Fe-19Mn alloy at low and high strain amplitude. Mater Sci Eng A. 2013;560:837. https://doi.org/10.1016/j.msea.2012.10.060

[9]Liu R, Sun HL, Liu XL, Yan WW, Jiang XS. Effect of Gd on microstructure, mechanical properties and damping properties of Fe-Cr-Al alloys. Mater Charact. 2022;187:111841. https://doi.org/10.1016/j.matchar.2022.111841

[10]Zhou ZC, Wen CE, Yang H, Yan YJ. Low frequency damping capacity in a strained Fe-Mn-Si alloy. Phys Status Solidi A. 2010;207(2):338. https://doi.org/ 10.1002/pssa.200925090

[11]Honga JS, Choi SM, Lee YK. Stasis mechanism of γ → ε martensitic transformation in Fe-17Mn alloy. Acta Mater. 2021;210:116846. https://doi.org/10.1016/j.actamat.2021.116846

[12]Chen J, Zhang WN, Liu ZY, Wang GD. Microstructural evolution and deformation mechanism of a Fe-15Mn alloy investigated by electron back-scattered diffraction and transmission electron microscopy. Mater Sci Eng A. 2017;698:198. http://doi.org/10.1016/j.msea.2017.05.059

[13]Kim GH, Nishimura Y, Watanabe Y, Sato H, Nishino Y, Jung HR, Kang CY, Kim IS. Effects of ε martensite and dislocations behavior by thermo-mechanical treatment on Fe-Cr-Mn damping alloy. Mater Sci Eng A. 2009;521-522:368. http://doi.org/10.1016/j.msea.2008.09.138

[14]Sun HY, Giron-Palomares B, Qu WH, Chen G, Wang H. Effects of Cr addition and cold pre-deformation on the mechanical properties, damping capacity, and corrosion behavior of Fe-17%Mn alloys. J Alloy Compd. 2019;803:250. https://doi.org/10.1016/j.jallcom.2019.06.178

[15]Wang HJ, Wang H, Zhang RQ, Liu R, Xu Y, Tang R. Effect of high strain amplitude and pre-deformation on damping property of Fe-Mn alloy. J Alloy Compd. 2019;770:252. https://doi.org/10.1016/j.jallcom.2018.08.099

[16]Yan N, Geng D, Wei BB. Damping performance and martensitic transformation of rapidly solidified Fe-17%Mn alloy. J Mater Sci Technol. 2002;117:1. https://doi.org/10.1016/j.jmst.2021.10.042

[17]Sun LY, Cheng WC, Balagurov AM, Bobrikov IA, Cifre J, Chudakov IB, Jen SU, Cheverikin VV, Zadorozhnyy MY, Golovin IS. Effect of thermal cycling on microstructure and damping capacity of Fe-26Mn-4Si alloy. Mater Charact. 2020;159:110001. https://doi.org/10.1016/j.matchar.2019.110001

[18]Chen G, Giron-Palomares B, Sun HY, Wang H, Zhang YY, Duan L, Wang J, Cao P. Effect of alloying with Al and Cr on the microstructure, damping capacity and high-temperature oxidation behaviors of Fe-17Mn damping alloys. J Alloy Compd. 2020;819:153035. https://doi.org/10.1016/j.jallcom.2019.153035

[19]Jun JH, Kong DK, Choi CS. The influence of Co on damping capacity of Fe-Mn-Co alloys. Mater Res Bull. 1998;33(10):1419. https://doi.org/10.1016/s0025-5408(98)00145-7

[20]Jun JH, Choi CS. The influence of Mn content on microstructure and damping capacity in Fe-(17-23)%Mn alloys. Mater Sci Eng A. 1998;252:133. https://doi.org/10.1016/s0025-5408(98)00145-7

[21]Chen LH, Li CR, Li ZY. Effect of rare earth Ce on martensite structure of Fe-Mn damping alloy. Mater Res Express. 2019;6(12):1265i4. https://doi.org/10.1088/2053-1591/ab6d2d

[22]Han Y, Liu ZH, Wu CB, Zhao Y, Zu GQ, Zhu WW, Ran X. A short review on the role of alloying elements in duplex stainless steels. Tungsten. 2023;5(4):419-439. https://doi.org/10.1007/s42864-022-00168-z

[23]Takaki S, Nakatsu H, Tokunaga Y. Effects of austenite grain size on ε martensitic transformation in Fe-15mass%Mn alloy. Mater Trans. 1993;34(6):489. https://doi.org/10.2320/matertrans1989.34.489

[24]Huang SK, Li N, Wen YH, Teng J, Ding S, Xu YG. Effect of Si and Cr on stacking fault probability and damping capacity of Fe-Mn alloy. Mater Sci Eng A. 2007;479(1-2):223. http://doi.org/10.1016/j.msea.2007.06.063

[25]Grässel O, Krüger L, Frommeyer G, Meyer LW. High strength Fe-Mn-(Al, Si) TRIP/TWIP steels development-properties-application. Int J Plasticity. 2002;16(10-11):1391. http://doi.org/10.1016/s0749-6419(00)00015-2

[26]Igata N. Applications of high damping stainless alloy (HIDAS). Key Eng Mater. 2009;319:209. http://doi.org/10.4028/www.scientific.net/kem.319.209

[27]Yang L, Jiang XS, Sun HL, Shao ZY, Fang YJ, Shu R. Effect of Ta addition on microstructures, mechanical and damping properties of Cu-Al-Mn-Ti alloy. J Mater Res Technol. 2021;15:3825. https://doi.org/10.1016/j.jmrt.2021.10.031

[28]Xu DF, Zhang HT, Wang ML, Lu YP, Chen XH, Ren Z. Enhanced strength-ductility synergy in a Ta-doped CoCrNi medium-entropy alloy with a dual heterogeneous structure. Mater Sci Eng A. 2022;860:144293. https://doi.org/10.1016/j.msea.2022.144293

[29]Yang HY, Wang Z, Shu SL, Lu JB. Effect of Ta addition on the microstructures and mechanical properties of in situ bi-phase (TiB_2-TiC_xN_y)/(Ni-Ta) cermets. Ceram. Int. 2019;45(4):4408. https://doi.org/10.1016/j.ceramint.2018.11.118

[30]Shoon DW, Kang CY, Miyahara K, Sung JH. Effect of microstructure on the damping capacity and strength in Fe-Al-Mn alloy. SAE Tech Pap. https://doi.org/10.4271/2004-01-0745

[31]He W, Luo Q, Peng HB, Wen YH. Remarkable improvement of damping capacity in FeMn-based alloys by a long annealing. Mater Sci Technol. 2020;36(12):1329. https://doi.org/10.1080/02670836.2020.1780002

[32]Pandey A, Dalal S, Dutta S, Dixit A. Structural characterization of polycrystalline thin films by X-ray diffraction technique. J Mater Sci. 2021;32:1341. https://doi.org/10.1007/s10854-020-04998-w

[33]Jiang HG, Rühle M, Lavernia EJ. On the applicability of the x-ray diffraction line profile analysis in extracting grain size and microstrain in nanocrystalline materials. J Mater Res. 1999;14(2):549. https://doi.org/10.1557/jmr.1999.0079

[34]Wang SN, Li Y, Zhao TT. Effect of thermal oxidation on the surface characteristics and corrosion behavior of a Ta-implanted Ti-50.6Ni shape memory alloy. Int J Min Met Mater. 2012;19(12):1134. https://doi.org/10.1007/s12613-012-0682-3

[35]Yang LL, Wang JL, Yang RZ, Yang SS, Jia YX, Chen MH, Qiao YX, Guo PY, Zhu SL, Wang FH. Oxidation behavior of a nanocrystalline coating with low Ta content at high temperature. Corros Sci. 2020;180:109182. https://doi.org/10.1016/j.corsci.2020.109182

[36]Cherian RP, Smith LN, Midha PS. A neural network approach for selection of powder metallurgy materials and process parameters. Artif Intell Eng. 2000;14(1):39. https://doi.org/10.1016/s0954-1810(99)00026-6

[37]Shu R, Jiang XS, Shao ZY, Sun DM, Zhu DG, Luo ZP. Fabrication and mechanical properties of MWCNTs and graphene synergetically reinforced Cu-graphite matrix composites. Powder Technol. 2019;349:59. https://doi.org/10.1016/j.powtec.2019.03.021
[38]Srinivasarao B, Oh-ishi K, Hono K. Microstructure and mechanical properties of Fe-C alloy produced by mechanical alloying and spark plasma sintering. J Phys Conf Ser. 2009;144:012026. https://doi.org/10.1088/1742-6596/144/1/012026
[39]Ya GD, Shang C, Nan NJ, Qiu HZ, Liang W, Yun FX, Ke J. Microstructures and mechanical properties of Ta–Nb–Zr–Ti–Al refractory high entropy alloys with varying Ta/Ti ratios. Tungsten. 2021;3(4):406-414. https://doi.org/10.1007/s42864-021-00111-8
[40]Xu WW, Han JJ, Wang ZW, Wang CP, Wen YH, Liua XJ, Zhu ZZ. Thermodynamic, structural and elastic properties of Co_3X (X=Ti, Ta, W, V, Al) compounds from first-principles calculations. Intermetallics. 2012;32:303. https://doi.org/10.1016/j.intermet.2012.08.022